N 1s RIXS of a Ru photosensitiser; understood through increasing the complexity from individual ligands to the complete molecule.

Robert H. Temperton,[1] Stephen Skowron,[2] Karsten Handrup,[3] Andrew J. Gibson,[1] Alessandro Nicolaou,[4] Nicolas Jaouen,[4] Elena Besley,[2] and James N. O'Shea[1, a)]

[1)] *School of Physics, University of Nottingham, Nottingham, NG7 2RD, UK*

[2)] *School of Chemistry, University of Nottingham, Nottingham, NG7 2RD, UK*

[3)] *Synchrotron Radiation Research, Department of Physics, Box 118, SE-221 00 Lund, Sweden*

[4)] *Synchrotron SOLEIL, Saint-Aubin, BP 48, 91192 Gif-sur-Yvette, France*

Understanding the resonant inelastic x-ray scattering (RIXS) of dye molecules provides a route to determining the frontier molecular orbital structure that underpins the function of dyes in light harvesting interfaces. We have measured N 1*s* RIXS maps of the dye molecule cis-bis(isothiocyanato)bis(2,2'-bipyridyl-4,4'-dicarboxylato)ruthenium(II), known as "N3", and of the isolated bipyridine-dicarboxylic acid ligand ("bi-isonicotinic acid") and the single ring analogue "isonicotinic acid". Further interpretation is provided through complementary resonant photoemission spectroscopy (RPES) and density functional theory calculations. Clear evidence for intermolecular hydrogen bonding in both the bulk/crystalline isonicotinic and bi-isonicotinic acid powders is observed, along with clear vibronic coupling features. For the dye complex we interpret the RIXS in terms of the orbtial contributions of the bi-isonicotinic acid and thiocyanate ligands and the projection of the partial densities of states onto the different nitrogen atoms. This confirms the localisation and relative coupling of the frontier orbitals, and associated vibrational losses.

I. INTRODUCTION

Ruthenium centred organometallic complexes have a range of applications in light harvesting devices such as dye sensitised solar cells (DSSCs)[1] and photoelectrochemical water splitting devices.[2] This study is focussed on the "N3" dye, cis-bis(isothiocyanato)bis(2,2'-bipyridyl-4,4'-dicarboxylic acid)ruthenium(II) also known as Ru535, which has become a benchmark molecule for use in DSSCs and has been previously studied using photoelectron spectroscopies on rutile titanium dioxide[3], gold[4,5] and aluminium oxide surfaces[6]. N3 bonds to oxide surfaces primarily through the carboxyl groups of the bi-isonicotinic acid (2,2'-bipyridyl-4,4'-dicarboxylic acid) ligands, which in turn is made up of two isonicotinic acid molecules (pyridine-4-carboxylic acid). These molecules, shown in Figure 1a, are also well-studied, where bi-isonicotinic acid in particular has proven to act as a model system of these dye sensitised devices, allowing investigation of the absorption, bonding and charge transfer dynamics between the ligand and surface.[7–11]

X-ray photoelectron spectroscopy (XPS) and X-ray absorption spectroscopy (XAS) highlight an interesting difference between the isonicotinic acid and bi-isonicotinic acid molecules with regards to the head-to-tail hydrogen bonding between the N atom of the pyridine ring and the OH group of the carboxyl group of neighbouring molecules. For multilayers of isonicotonic acid, hydrogen bonding has been shown to produce a core level shift in the XPS and an additional state in the XAS.[12,13] For bi-isonicotinic acid, we believe no conclusive evidence of hydrogen bonding has been observed for multilayers of the molecule on a surface despite the fact that in the bulk crystal structure, each carboxylic acid group is hydrogen bonded to the pyridine nitrogen in a neighbouring molecule as illustrated in Figure 1b. In this crystal structure, the bi-isonicotinic acid molecules are arranged in two-dimensional sheets participating in both head-to-tail hydrogen bonding and face-to-face $\pi \cdots \pi$ interactions.[14] Similarly, the crystal structure of isonicotinic acid shows linear chains of head-to-tail hydrogen-bonded molecules.[15]

Resonant inelastic x-ray scattering (RIXS) can provide atom-specific information about the occupied and unoccupied valence orbitals of a molecule and the coupling between them.[16] It is therefore an ideal probe of molecular electronic structure, which underpins electron dynamics and thus solar energy conversion mechanisms in molecular systems.[17] RIXS also provides a sensitive probe of molecular interactions such as hydrogen-bonding.[18,19] In RIXS the unoccupied molecular orbitals are populated by excitation of a core-electron through the absorption of a photon tuned to a specific resonance producing a core-excited state. The de-excitation step proceeds from either the populated state (elastic scattering), or from an occupied valence state (inelastic scattering). The inelastic scattering projects the partial density of valence states onto the core-level and is governed by the dipole selection rule. In our case, by tuning the absorption energy for excitation of an N 1*s* electron into the lowest unoccupied molecular orbitals (LUMOs) of each molecule, we therefore probe the unoccupied N 2*p*-derived orbitals. In this paper we present two-dimensional N 1*s* RIXS maps of isonicotinic acid, bi-isonicotinic acid and N3 in their bulk crystalline form. This represents a systematic increase in complexity from the simplest pyridine carboxylic acid ligand to the ruthenium dye complex. In addition, for N3,

[a)] Electronic mail: J.Oshea@nottingham.ac.uk

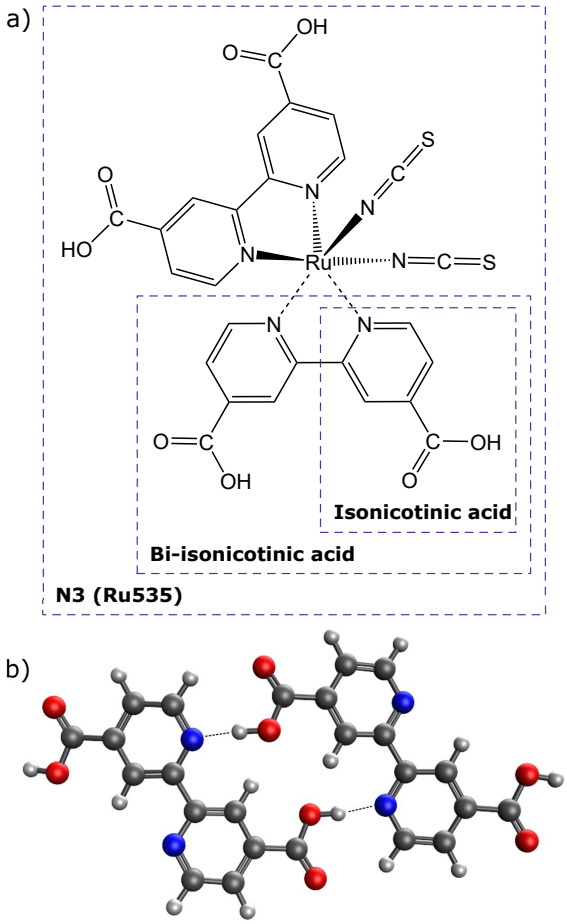

FIG. 1. a) Schematic illustration of the chemical structures of the N3 dye complex, its bi-isonicotinic acid ligands, and the single pyridine ring analogue isonicotinic acid. b) Calculated geometry of the hydrogen-bonding motif of bi-isonicotinic acid known from x-ray diffraction to be present in the crystal structure.

we compare the RIXS to resonant photoemission electron spectroscopy (RPES), which is the non-radiative compliment to RIXS that also allows observation of the coupling between occupied and unoccupied states. For bi-isonicotonic acid, we compare the bulk crystalline powder RIXS to that of a thick multilayer film physisorbed on a surface to highlight differences in the intermolecular interactions in these two phases.

II. METHODS

A. Experimental

Resonant inelastic x-ray scattering (RIXS) measurements were performed using the AERHA (adjustable energy resolution high acceptance) spectrometer[20] at the Sextants beamline[21] at Synchrotron Soleil in France. Bulk/powder samples were made by pressing the bulk crystalline powder of N3 (Solaronix), bi-isonicotinic acid (Alfa Aesar) and isonicotinic acid (Sigma Aldrich) onto graphite tape. Multilayer bi-isonictinic acid samples were prepared in a separate ultra-high vacuum (UHV) system in our home laboratory equipped with a Scienta R3000 analyser and dual anode (Al Kα, Mg Kα) X-ray source. Substrates were rutile TiO_2(110) single crystals (Pi-Kem, UK) cleaned by repeated cycles of argon ion sputtering (2 kV followed by 1 kV), and annealing in UHV to ∼900 K until no C 1s signal was detected in the XPS. Multilayers of bi-isonicotinic acid, were deposited onto the prepared substrates held at room temperature by sublimation from a Knudsen-type cell evaporation source (at ∼500 K) until no Ti 2p signal was detected in the XPS. The multilayer samples were then transported to Soleil and transferred into the analysis chamber of the Sextants beamline where the base pressure was 1×10^{-9} mbar.

The incident beam at Sextants is focused to a spot size of 2(v) μm × 100(h) μm. To prevent beam damage of the molecules, the sample was continuously moved during the measurements at a rate such that no changes were observed in concurrent spectra. The emitted photon energy scale of the RIXS spectrometer was calibrated by measuring the elastic peak at 5 eV increments across the whole detector range using linear vertical polarization of the incoming beam to maximise the elastic (Rayleigh) scattering intensity. For the RIXS maps and XAS over the N 1s absorption edge the beam was linearly polarized in the horizontal plane (in the plane of the spectrometer) and an incidence angle of 35˚ with respect to the surface. The overall measurement resolution was set to 300 meV (compared to the optimum resolution of 110 meV) as a compromise between energy resolution and spectrometer transmission. The RIXS maps are constructed from x-ray emission spectra measured for 10 minutes at each absorption energy.

Resonant photoemission spectroscopy (RPES) of N3 was carried out at beamline I511 on the MAX-II ring at the former MAX-Lab synchrotron radiation facility (now MAX-IV). This previously unpublished data was collected as part of the study presented by Mayor et al. in 2008[3] where details about the measurements can be found with the exception that the multilayer N3 sample was prepared *ex-situ* by electrospray deposition in low vacuum (whereas Mayor's paper presents *in-situ* deposits in high vacuum). Again, a rutile TiO_2(110) single crystal was used as a substrate prepared as described above prior to being removed from the UHV preparation chamber for the deposition. After the deposition, the sample was transferred immediately back into the UHV system for the measurements.

B. Computational

Density functional theory (DFT) calculations were performed using the Q-Chem 5.0 quantum chemistry software package[22], using the B3LYP exchange-correlation

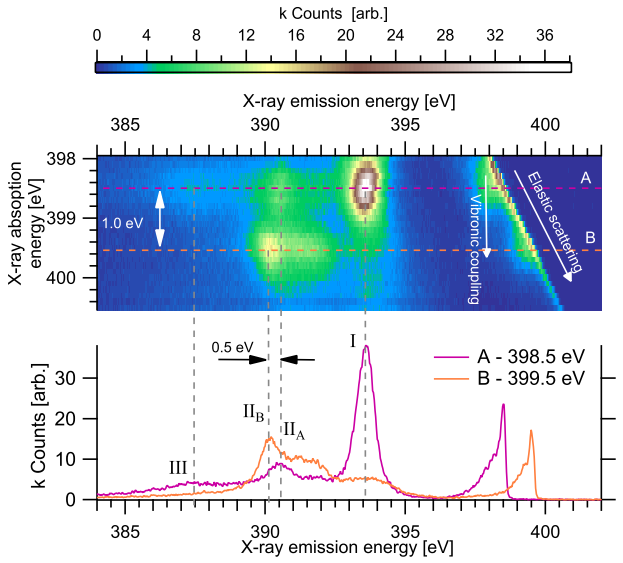

FIG. 2. N 1*s* RIXS map for the isonicotinic acid crystalline powder. The features observed below 397 eV emission energy are attributed inelastic scattering and those above 397 eV emission energy to elastic (Rayleigh) scattering and small inelastic losses due to vibronic coupling.

functional[23,24] and a 6-311G* basis set for all atoms other than ruthenium, and the the SRSC effective core potential (ECP)[25] for the core orbitals of the ruthenium atom. The N3 molecule geometry was optimised at this level of theory using an SCF convergence criterion of 10^{-8} and a cutoff of 10^{-10} for the neglect of two electron integrals, and molecular orbitals were plotted using an isovalue of 0.04 electrons/bohr^3. DFT calculations of the hydrogen bonding motif of bi-isonicotinic acid (Figure 1b) included an empirical dispersion correction via the Grimme BJ-damping model DFT-D3(BJ).[26]

III. RESULTS & DISCUSSION

A. Isonicotinic acid

The N 1*s* RIXS map measured for the isonicotinic acid (see Figure 1a) crystalline powder is shown in Figure 2a. Elastic scattering gives rise to a narrow feature that disperses linearly in emission energy as the absorption energy increases. At an absorption energy of 398.6 eV there is a strong enhancement in the intensity just below the elastic line and strong inelastic scattering features observed below ∼395 eV emission energy. This absorption (A) is attributed to excitation from the N 1*s* core-level into the LUMO-derived state of the core-excited molecule. This is consistent with previous electron yield XAS measurements for multilayer films of isonicotinic acid deposited on titanium dioxide surfaces.[12,13] The intensity observed to the low emission energy side of the elastic line does not disperse linearly with the elastic line but instead is observed at an almost constant emission energy of 398 eV. This corresponds to radiative decay of the core-hole always from the same vibrational component of the core-excited state. While the absorption energy is tuned over the LUMO-derived resonance (A), dissipation of the vibrational energy results in the decay proceeding from the lowest accessible state. This feature is therefore attributed to vibronic coupling.[27] The main feature of the inelastic scattering at resonance A is the strong enhancement of feature I at an emission energy of 393.6 eV. This is attributed to radiative decay from the highest occupied molecular orbital (HOMO). Weaker enhancements are observed at energies of 390.4 eV (II_A) and 387.5 eV (III) attributed to decay from lower energy molecular orbitals (the matrix element). The inelastic scattering represents the partial density of states of the molecule modulated by the coupling between the occupied and unoccupied molecular orbitals involved. The strong enhancement of peak I at resonance A is therefore attributed to strong coupling between the HOMO and LUMO, while peaks II_A and III have a relatively weaker coupling with the LUMO.

At an absorption energy of 399.5 eV a second band of enhancements (B) is observed both on the lower emission energy side of the elastic line and within the manifold of inelastic scattering. The intensity just below the elastic line is again attributed to vibronic coupling as for the LUMO. In this case the vibronic emission is observed at an almost constant energy of 399.2 eV. The separation between the main absorption energy and the vibronic line is 0.3 eV for resonance B compared with 0.5 eV for resonance A. This difference is attributed to the different character of this molecular orbital, which is further illustrated by the inelastic scattering. At the absorption energy of resonance B, the strongest enhancement is observed at an emission energy of 390.2 eV (II_B) and a broad shoulder extending up to 391.2 eV. An absorption similar to resonance B has previously been observed in the electron yield XAS of multilayers of isonicotinic acid deposited on a titanium dioxide surface.[12,13] This resonance was shown to be highly dependent on the growth conditions of the film, and attributed to hydrogen-bonding between the carboxylic group of one molecule and the N atom of the pyridine ring of a neighbouring molecule, that form only when the molecules are deposited at a very slow rate. In the XAS multilayer studies[12,13] the separation of resonances A and B was 1.2 eV, compared to 1.0 eV in the RIXS results shown in Figure 2 for the crystalline powder. Since the crystal structure of isonicotinic acid is known to be hydrogen bonded, we attribute resonance B to a new LUMO state arising from this N···OH hydrogen bond interaction, with the small difference in energy likely due to the slightly different bonding environment in the bulk crystal compared with the physisorbed multilayer.

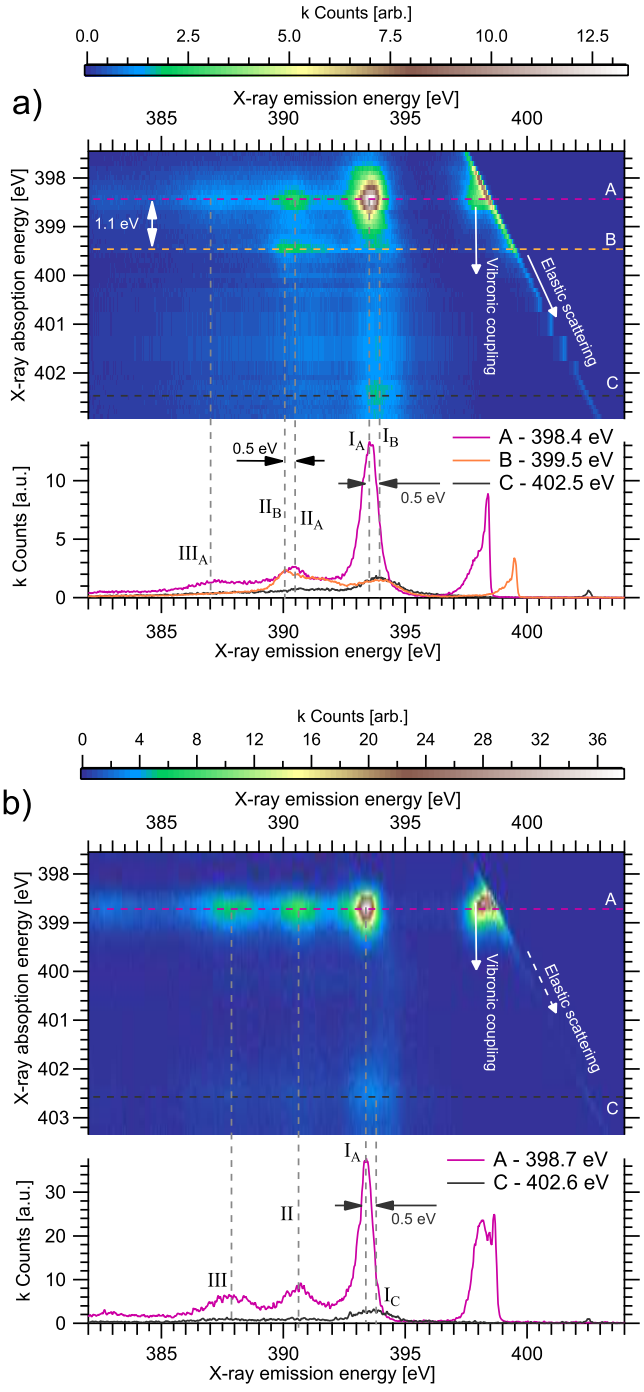

FIG. 3. Bi-isonicotinic acid N 1*s* RIXS maps of a) crystalline powder and b) physisorbed multilayer. Below each are line profiles extracted for key resonant transitions.

B. Bi-isonicotinic acid

The N 1*s* RIXS map measured for the bi-isonicotinic acid (see Figure 1a) crystalline powder is shown in Figure 3a. The RIXS data for the bi-isonicotinic acid powder exhibits similar features to isonicotinic acid, which is largely expected due to the similarity of the molecular structures. We find the first absorption resonance at an absorption energy of 398.4 eV (A) where we again observe inelastic scattering involving the occupied molecular orbitals below an emission energy of around 395 eV. The strongest of these (I_A) appears at an emission energy of 393.5 eV attributed as for isonicotic acid to the HOMO. Weaker features are observed at 390 eV (II_A) and 387 eV (III_A) attributed to decay from lower lying molecular orbtials. Resonance A is attributed to the LUMO and while this appears at a slightly different absorption energy compared to isonicotonic acid, we find the resulting inelastic scattering to bear a striking similarity with the single ring molecule.

At an absorption of 399.5 eV photon energy a second band of enhancements (B) is observed both on the lower emission energy side of the elastic line and within the manifold of inelastic scattering. Similar to isonicotinic acid, we find a much weaker intensity for peak I_B. This peak is also shifted slightly to higher emission energy (394.0 eV). Peak II_B is observed at a similar intensity to II_A but shifted in the other direction to lower emission energy. We note that the II_A–II_B shift is 0.5 eV for both bi-isonicotinic and isonicotinic acids. The absorption energy separation of resonances A and B is 1.0 eV which is consistent with the corresponding separation for isonicotinic acid, and we again attribute resonance B to intermolecular N···OH hydrogen bonding in the bulk crystalline powder. The next resonance, labelled C, occurs at an absorption energy of 402.6 eV. This couples with a state at the same energy as the I_B feature centred at 394.0 eV.

The N 1*s* RIXS map measured for multilayer bi-isonicotinic acid physisorbed on TiO_2(110) is shown in Figure 3b. This data has been published previously[27] but is reproduced here in the same format as the powder data for direct comparison. Many spectral features are similar: the emission spectra on resonance A has features I, II and III appearing at the same energies and both have the same 0.5 eV shift between the HOMO enhancement at the A and C resonances. The key difference between the powder and the multilayer is the absence of resonance B in the physisorbed multilayer. This we attribute to the lack of hydrogen bonding between the molecules in the multilayer prepared by thermal evaporation. This is consistent with XPS, XAS and RPES measurements of bi-isonicotinic acid physisorbed multilayers where no evidence of hydrogen bonding has been observed.[11,12]. Compared to the power sample, features II and III in the multilayer are also more intense relative to feature I, which is also likely a result of the lack of hydrogen bonding.

For both the powder and the multilayer, the intensity observed at resonance A on the lower emission energy side of the elastic line is attributed to vibronic coupling (as for isonicotinic acid) which is discussed in detail elsewhere.[28] Here we note that this relative intensity of the vibronic feature is much stronger for the multilayer compared with

the bulk powder, where the vibronic coupling is most likely suppressed by the effect of the extended crystal structure mediated by the N···OH hydrogen bonding.

C. N3 dye

1. Calculated molecular orbitals

The molecular orbital and electronic structure of the N3 molecule is well understood - for a thorough computational analysis we would point the reader to the DFT study by Monat et al.[29] However, in order to aid discussion here, schematics showing localisation of relevant molecular orbitals are included in Figure 4. We would like to stress that these ground state DFT calculations are not intended to be an extensive simulation of the molecule's electronic properties in the context of this experiment - important details such as the effects of the core-hole are not included - but the calculations are intended to give readers not familiar with the molecule an insight into the orbital localisation.

The three occupied molecular orbitals shown in Figure 4, orbital numbers 163 (HOMO), 158 and 156, are all good representations of their surrounding orbitals with nearby energies. Orbitals 163-160 are mainly localised on the thiocyanate ligands and Ru atom. For orbitals 159-157 we see some density start to shift to the bi-isonicotonic acid ligands. By orbital 156 the density is localised almost exclusively on the bi-isonicotinic acid. The LUMO (orbital 164) is largely localised on the bi-isonicotonic acid ligands and the Ru center. With the exception of the LUMO+1 (orbital 165), which is distributed over the entire molecule, we don't see any notable density on the thiocyanate ligand until we reach orbital 175. When we reach orbital 188, we see the orbital is localised almost exclusively on the thiocyanate ligands.

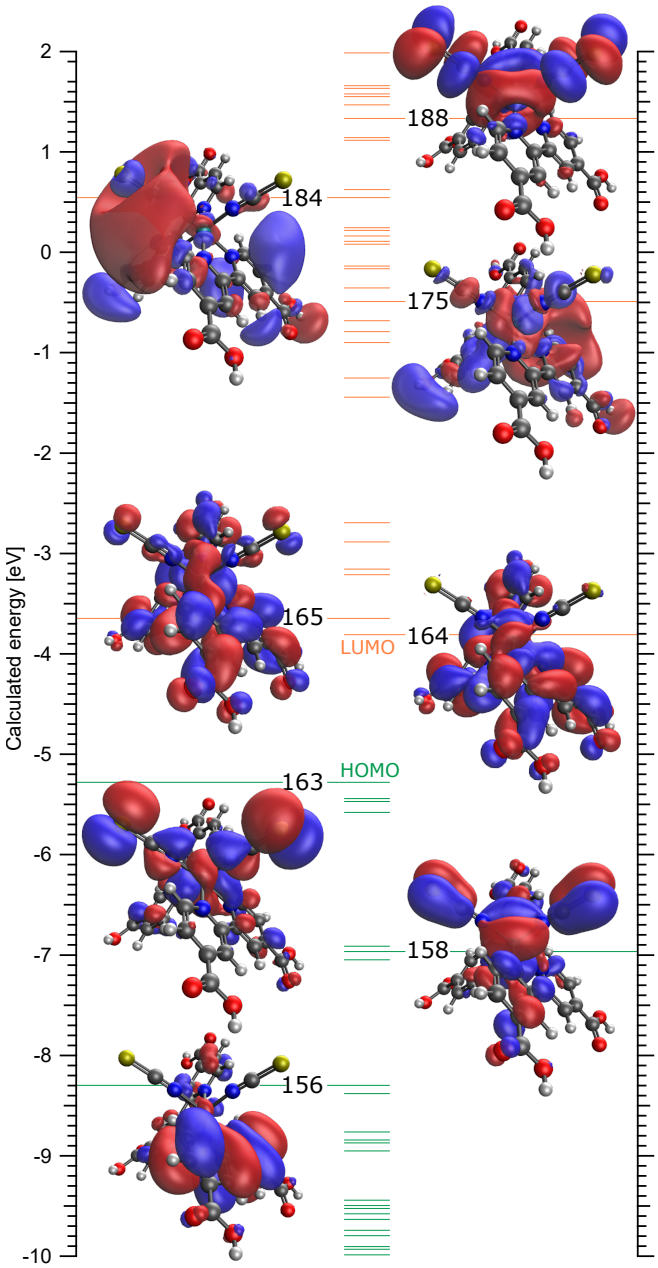

FIG. 4. Energies of occupied (green) and unoccupied (orange) molecular orbitals from ground state DFT calculations of an isolated N3 molecule. The localisation of orbitals 156 (−8.30 eV), 158 (−6.97 eV), 163 (HOMO, −5.28 eV), 164 (LUMO, −3.81 eV), 164 (−3.65 eV), 175 (−0.49 eV), 184 (+0.54 eV) and 188 (+1.33 eV) is shown.

2. RIXS Data

The N 1s RIXS map measured for the N3 dye (see Figure 1a) powder is shown in Figure 5. The first resonance (A) representing excitation into the LUMO is observed at an absorption energy centred around 399.2 eV. The inelastic scattering at this resonance exhibits a weak feature at 395 eV (II_A) emission energy and an intense feature at 393 eV (III_A), followed by a series of decreasing intensity peaks at 391, 389 and 384 eV. A second resonance (B) is observed 0.7 eV higher at 399.9 eV absorption energy. Here we observe a feature at 395 eV (I) in the inelastic scattering, but effectively no intensity at the emission energy of feature III_A. The data also shows a low intensity feature at emission energy ∼394 eV - the higher energy side of Feature I (on resonance B).

The intensity just below the elastic line at resonance A in the RIXS map is attributed, as for the isonicotinic and bi-isonicotinic acid molecules, to vibronic coupling and is observed at an almost constant emission energy as the absorption is tuned over the LUMO-derived resonance. There is no obvious vibronic peak observed at resonance B, which is possibly due to the very different nature of the thiocyanate ligands compared with the bi-isonicotinic acid ligands. Interestingly, while the vibronic

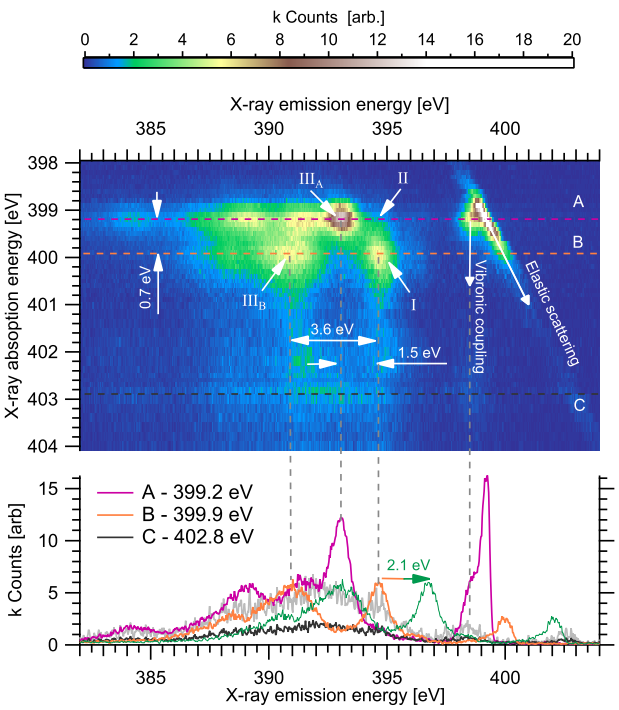

FIG. 5. N 1*s* RIXS of N3 dye (bulk powder sample). Line profiles A (purple) and B (orange) have been extracted from the map and represent excitation of the nitrogen atoms in the bi-isonicotinic acid and thiocyanate ligands respectively. Line profile C (black) has also been extracted - the light grey line shows this with the intensity multiplied by 3. The green line shows profile B shifted by 2.1 eV (the binding energy difference between the two N 1*s* core levels).

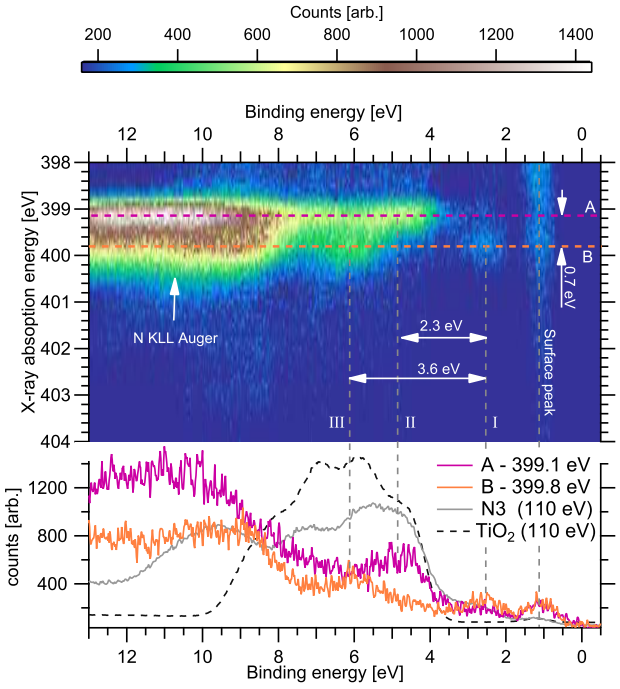

FIG. 6. N 1*s* RPES for an N3 multilayer. Line profiles A and B are again extracted representing excitation into the bi-isonicotinic acid and NCS ligands. These are compared to valence band XPS of the same sample of N3 (solid grey line) and the clean titanium dioxide surface surface (dashed black line). Features I, II and III correspond to the same occupied molecular orbitals features highlighted in the RIXS (Figure 5)

feature is not observed for resonance B, it reappears as a weak feature between 401.5 eV and 403.5 eV absorption energy (centred around absorption C at 402.8 eV). The inelastic scattering in this region suggests that these unoccupied molecular orbtials are distributed across the whole molecule, exhibiting features characteristic of both resonance A and B. The vibronic feature, however, results from a core-hole decay process originating from the lowest vibrational state of the LUMO. For this feature to be observed for these higher-lying states this could imply a two-step decay process where the photoexcited electron first decays from these higher unoccupied orbitals to the LUMO before filling the N 1*s* core-hole (in the timescale of the core-hole lifetime).

3. RPES Data

Further insight into the core-excited state of N3 can be obtained from the N 1*s* resonant photoemission (RPES), presented in Figure 6. This technique is the non-radiative analogue of RIXS and involves the same core-excited intermediate state. Also presented in Figure 6 are direct photoemission spectra of the valance band of the N3 multilayer and the underlying TiO_2(110) surface for comparison.

As discussed for the RIXS map, resonance B at an absorption energy of 399.8 eV is predominantly located on the thiocyanate ligands. Here we observe a participator enhancement (I) at a binding energy of 2.5 eV. This corresponds to a resonant enhancement of the HOMO of N3. A second enhancement (III) is observed at this resonance at a binding energy of 6.1 eV. The separation of 3.6 eV is identical to that presented in the RIXS (Figure 5) supporting our assignment of this feature.

Resonance A - attributed largely to the bi-isonicotinic acid ligands, is observed at an absorption energy of 399.1 eV. Here we observe only a weak resonant enhancement of the HOMO at a binding energy of 2.5 eV (I), and a stronger enhancement of a feature just below 5 eV. This feature (II) is attributed to the next experimentally distinct occupied molecular orbital. This feature is not enhanced at resonance B, suggesting that this orbital is localised on the bi-isonicotinic acid ligands. Returning to the RIXS map (Figure 5) we can now associate the weak intensity observed at 395 eV at resonance A (feature II) with this same occupied orbital.

The vertical, constant binding energy bands of intensity observed in the N 1*s* RPES map in Figure 6 are

due to direct photoemission of the valence states of the molecule and the underlying surface and contribute only a background of slowly decreasing intensity (due to decreasing cross section with increasing photon energy). Our assignments of molecule and surface features are consistent with valence band XPS (measured at 110 eV photon energy) of the N3 deposit and the underlying clean TiO_2(110) surface which are included in the figure for reference. The structure of the surface valence band matches well with the pre-absorption edge features visible in the map.

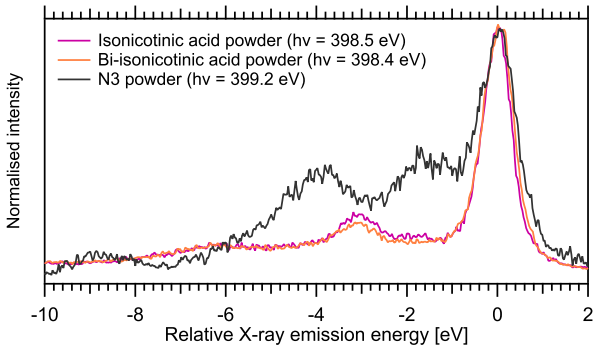

FIG. 7. N 1s RIXS emission spectra for all three powder samples measured on the LUMO resonances. The energy axis is relative to the position of the pyridine nitrogen's HOMO. Spectra are normalised to the height of this HOMO.

4. Discussion

We first note that N···OH hydrogen bonding is not possible for the N3 dye complex as all the nitrogen atoms are bonded to the central ruthenium atom. Therefore resonance B, unlike isonicotinic and bi-isonicotinic acid, cannot be attributed to intermolecular hydrogen bonding. Feature I is not observed at all in the RIXS of bi-isonicotinic acid and is assigned to the HOMO of N3. As shown by our DFT calculations (Figure 4) the HOMO is located predominantly on the thiocyanate ligands, while the LUMO is located largely on the bi-isonicotinic acid ligand. We would therefore expect a weak coupling to the HOMO at the LUMO-resonance (A), which is consistent with the RIXS and RPES maps. Resonance B, on the other hand, is therefore attributed to excitation into higher unoccupied molecular orbitals localised largely on the thiocyanate ligands.

In the DFT we dont see see substantial density appearing on the thiocyanate until we reach orbital 184, 4.35 eV above the LUMO. However, in the RIXS and RPES we see a separation of 0.7 eV between the two resonances. This can be understood by considering that the resonant transitions are dependent on both the energy of the core level and the unoccupied level. Core-level photoemission spectroscopy of N3 has shown the N 1s environment in the thiocyanate appears 2.1 eV lower in binding energy than that in the pyridine ring of the bi-isonicotinic acid ligand.[3] Therefore, the experimental data implies the unoccupied molecular orbitals on the thiocyanate actually lies 0.7 eV+2.1 eV= 2.8 eV above the LUMO. Although this is a still lower than the calculated separation, one has to remember the experiments measure decay processes from a core-excited state - the effects of the core-hole should be considered carefully if one wanted to precisely simulate X-ray absorption experiments.

For resonant photoemission (RPES), interpretation of the binding energy axis is trivial as it is not dependent on the photon or core-level energies - participator decay in RPES leaves the atom in a final state identical to that of normal photoemission of the occupied molecular orbital. For RIXS however, the measured photon is produced by filling the core hole - the binding energy of which therefore needs to be considered. In this case, the RIXS spectra are therefore a projection of the molecule's partial density of states onto the two different nitrogen core level environments, so we again need to consider the 2.1 eV energy difference between these core levels. The separation of peaks I and III_A in the RIXS map is 1.5 eV emission energy, which therefore translates into a binding energy difference of 3.6 eV. This is consistent with the separation of the features in the valence band photoemission, shown in Figure 6, which supports this interpretation. Moreover, if peak III_B (in the RIXS) is shifted to higher emission energy by 2.1 eV as required by this interpretation (shown in Figure 5), its emission energy coincides with peak III_A identifying both peaks as the same occupied molecular orbital. This can also be realised by the observation that the emission energy separation of peaks I and III_B is indeed 3.6 eV.

The features attributed to experimentally distinct occupied molecular orbitals (I, II and III) match well with the first three groupings of calculated occupied molecular orbitals (see Figure 4), represented by orbitals 163 (HOMO), 158 and 156 . Specifically orbitals 158 and 156 appear 1.7 eV and 3.0 eV below the HOMO which is a close match in relative energies considering the nature of the calculations.

Despite the complexities in the analysis of the RIXS where the core-level needs to be considered, we are still able to compare the shape of the emisssion spectra measured on the LUMO resonance for all three molecules relative to the HOMO on the pyridine (differences in core level positions would manifest as a shift in emission energy). This is presented in Figure 7 with the spectra normalised to the pyridine HOMO, the energy of which also defines "0 eV". When comparing the isonicotinic acid and bi-isonicotinic powders we see very similar structures. This is not surprising given the similarity of the two molecules. However when compared to the N3, we see that although the ligand is the same, the electronic structure is very different; the features are broader and appear at different relative energies. Again, this is not surprising as the environment is very different (the nitrogen has an additional ruthenium bond). This shows that

one has to take great care when using N 1s based transitions in bi-isonicotinic acid as a model system for N3, or similar complexes with this common anchoring ligand. It also highlights the value of RIXS to study these systems. Despite the much simpler binding energy axis in RPES, making this type of comparison would be much more challenging due to the strong N KLL Auger feature that overlaps the participant enhancements of the molecular orbitals, especially when considering weak features ∼10 eV below the HOMO.

IV. CONCLUSIONS

We have measured N 1s RIXS maps of the dye molecule cis-bis(isothiocyanato)bis(2,2'-bipyridyl-4,4'-dicarboxylic acid)ruthenium(II) and of the isolated ligand bi-isonicotinic acid and the single ring analogue isonicotinic acid in the bulk powder. For both the isonicotinic and bi-isonicotinic acid in the bulk crystalline powder form we see direct evidence of hydrogen bonding in the form of a resonant transition at 399.5 eV absorption energy. This assignment was aided by comparison to a physisorbed multilayer where hydrogen bonding is not present. For the bulk powder, we also see evidence of vibronic coupling but note the features are less intense than observed in the multilayer. For the N3 dye complex we interpret the RIXS in terms of the orbtial contributions of the bi-isonicotinic acid and thiocyanate ligands and the projection of the partial densities of states onto the different nitrogen atoms. Further interpretation is provided through comparison with resonant photoemission spectroscopy (RPES) and density functional theory (DFT) calculations highlighting the usefulness of combining these three complimentary techniques for understanding the electronic structure of complex molecules. This analysis allowed us to confirm the localisation and relative coupling of the frontier orbitals and associated vibrational losses for this important photosensitiser complex.

V. REFERENCES

[1] M. Grätzel, Journal of Photochemistry and Photobiology C: Photochemistry Reviews **4**, 145 (2003).

[2] J. J. Concepcion, J. W. Jurss, M. K. Brennaman, P. G. Hoertz, A. O. T. Patrocinio, N. Y. Murakami Iha, J. L. Templeton, and T. J. Meyer, Accounts of Chemical Research **42**, 1954 (2009).

[3] L. C. Mayor, J. Ben Taylor, G. Magnano, A. Rienzo, C. J. Satterley, J. N. O'Shea, and J. Schnadt, The Journal of chemical physics **129**, 114701 (2008).

[4] L. C. Mayor, A. Saywell, G. Magnano, C. J. Satterley, J. Schnadt, and J. N. O'Shea, Journal of Chemical Physics **130** (2009), 10.1063/1.3122685.

[5] A. J. Britton, M. Weston, J. B. Taylor, A. Rienzo, L. C. Mayor, and J. N. O'Shea, The Journal of chemical physics **135**, 164702 (2011).

[6] A. J. Gibson, R. H. Temperton, K. Handrup, M. Weston, L. C. Mayor, and J. N. O'Shea, The Journal of chemical physics **140**, 234708 (2014), arXiv:1407.5186.

[7] J. B. Taylor, L. C. Mayor, J. C. Swarbrick, J. N. O'Shea, C. Isvoranu, and J. Schnadt, The Journal of chemical physics **127**, 134707 (2007).

[8] L. Patthey, H. Rensmo, P. Persson, K. Westermark, L. Vayssieres, A. Stashans, A. Petersson, P. A. Bruhwiler, H. Siegbahn, S. Lunell, and N. Martensson, The Journal of Chemical Physics **110**, 5913 (1999).

[9] P. Persson, S. Lunell, P. A. Brühwiler, J. Schnadt, S. Södergren, J. N. O'Shea, O. Karis, H. Siegbahn, N. Mårtensson, M. Bässler, and L. Patthey, The Journal of Chemical Physics **112**, 3945 (2000).

[10] J. Schnadt, A. Henningsson, M. P. Andersson, P. G. Karlsson, P. Uvdal, H. Siegbahn, P. A. Bruhwiler, and A. Sandell, The Journal of Physical Chemistry B **108**, 3114 (2004).

[11] R. Temperton, A. Gibson, K. Handrup, and J. O'Shea, Journal of Chemical Physics **147** (2017), 10.1063/1.4996746.

[12] J. O'Shea, Y. Luo, J. Schnadt, L. Patthey, H. Hillesheimer, J. Krempasky, D. Nordlund, M. Nagasono, P. Brühwiler, and N. Mårtensson, Surface Science **486**, 157 (2001).

[13] J. N. O'Shea, J. Schnadt, P. A. Brühwiler, H. Hillesheimer, N. Mårtensson, L. Patthey, J. Krempasky, C. Wang, Y. Luo, and H. Ågren, The Journal of Physical Chemistry B **105**, 1917 (2001).

[14] E. Tynan, P. Jensen, P. E. Kruger, A. C. Lees, and M. Nieuwenhuyzen, Dalton Transactions **117**, 1223 (2003).

[15] F. Takusagawa and A. Shimada, Acta Crystallographica Section B Structural Crystallography and Crystal Chemistry **32**, 1925 (1976).

[16] T. Schmitt, F. M. F. de Groot, and J.-E. Rubensson, Journal of Synchrotron Radiation **21**, 1065 (2014).

[17] C. S. Ponseca, P. Chábera, J. Uhlig, P. Persson, and V. Sundström, Chemical Reviews **117**, 10940 (2017).

[18] V. Vaz da Cruz, F. Gel'mukhanov, S. Eckert, M. Iannuzzi, E. Ertan, A. Pietzsch, R. C. Couto, J. Niskanen, M. Fondell, M. Dantz, T. Schmitt, X. Lu, D. McNally, R. M. Jay, V. Kimberg, A. Föhlisch, and M. Odelius, Nature Communications **10**, 1 (2019).

[19] L. Weinhardt, E. Ertan, M. Iannuzzi, M. Weigand, O. Fuchs, M. Bär, M. Blum, J. D. Denlinger, W. Yang, E. Umbach, M. Odelius, and C. Heske, Physical Chemistry Chemical Physics **17**, 27145 (2015).

[20] S. G. Chiuzbăian, C. F. Hague, A. Avila, R. Delaunay, N. Jaouen, M. Sacchi, F. Polack, M. Thomasset, B. Lagarde, A. Nicolaou, S. Brignolo, C. Baumier, J. Lüning, and J. M. Mariot, Review of Scientific Instruments **85** (2014), 10.1063/1.4871362.

[21] M. Sacchi, N. Jaouen, H. Popescu, R. Gaudemer, J. M. Tonnerre, S. G. Chiuzbaian, C. F. Hague, A. Delmotte, J. M. Dubuisson, G. Cauchon, B. Lagarde, and F. Polack, Journal of Physics: Conference Series **425**, 072018 (2013).

[22] Y. Shao, Z. Gan, E. Epifanovsky, A. T. Gilbert, M. Wormit, J. Kussmann, A. W. Lange, A. Behn, J. Deng, X. Feng, D. Ghosh, M. Goldey, P. R. Horn, L. D. Jacobson, I. Kaliman, R. Z. Khaliullin, T. Kuś, A. Landau, J. Liu, E. I. Proynov, Y. M. Rhee, R. M. Richard, M. A. Rohrdanz, R. P. Steele, E. J. Sundstrom, H. L. Woodcock, P. M. Zimmerman, D. Zuev, B. Albrecht, E. Alguire, B. Austin, G. J. O. Beran, Y. A. Bernard, E. Berquist, K. Brandhorst, K. B. Bravaya, S. T. Brown, D. Casanova, C.-M. Chang, Y. Chen, S. H. Chien, K. D. Closser, D. L. Crittenden, M. Diedenhofen, R. A. DiStasio, H. Do, A. D. Dutoi, R. G. Edgar, S. Fatehi, L. Fusti-Molnar, A. Ghysels, A. Golubeva-Zadorozhnaya, J. Gomes, M. W. Hanson-Heine, P. H. Harbach, A. W. Hauser, E. G. Hohenstein, Z. C. Holden, T.-C. Jagau, H. Ji, B. Kaduk, K. Khistyaev, J. Kim, J. Kim, R. A. King, P. Klunzinger, D. Kosenkov, T. Kowalczyk, C. M. Krauter, K. U. Lao, A. D. Laurent, K. V. Lawler, S. V. Levchenko, C. Y. Lin, F. Liu, E. Livshits, R. C. Lochan, A. Luenser, P. Manohar, S. F. Manzer, S.-P. Mao, N. Mardirossian, A. V. Marenich, S. A. Mau-

rer, N. J. Mayhall, E. Neuscamman, C. M. Oana, R. Olivares-Amaya, D. P. O'Neill, J. A. Parkhill, T. M. Perrine, R. Peverati, A. Prociuk, D. R. Rehn, E. Rosta, N. J. Russ, S. M. Sharada, S. Sharma, D. W. Small, A. Sodt, T. Stein, D. Stück, Y.-C. Su, A. J. Thom, T. Tsuchimochi, V. Vanovschi, L. Vogt, O. Vydrov, T. Wang, M. A. Watson, J. Wenzel, A. White, C. F. Williams, J. Yang, S. Yeganeh, S. R. Yost, Z.-Q. You, I. Y. Zhang, X. Zhang, Y. Zhao, B. R. Brooks, G. K. Chan, D. M. Chipman, C. J. Cramer, W. A. Goddard, M. S. Gordon, W. J. Hehre, A. Klamt, H. F. Schaefer, M. W. Schmidt, C. D. Sherrill, D. G. Truhlar, A. Warshel, X. Xu, A. Aspuru-Guzik, R. Baer, A. T. Bell, N. A. Besley, J.-D. Chai, A. Dreuw, B. D. Dunietz, T. R. Furlani, S. R. Gwaltney, C.-P. Hsu, Y. Jung, J. Kong, D. S. Lambrecht, W. Liang, C. Ochsenfeld, V. A. Rassolov, L. V. Slipchenko, J. E. Subotnik, T. Van Voorhis, J. M. Herbert, A. I. Krylov, P. M. Gill, and M. Head-Gordon, Molecular Physics **113**, 184 (2015).

[23] A. D. Becke, The Journal of Chemical Physics **98**, 5648 (1993).

[24] P. J. Stephens, F. J. Devlin, C. F. Chabalowski, and M. J. Frisch, The Journal of Physical Chemistry **98**, 11623 (1994).

[25] D. Andrae, U. Häußermann, M. Dolg, H. Stoll, and H. Preuß, Theoretica Chimica Acta **77**, 123 (1990).

[26] S. Grimme, S. Ehrlich, and L. Goerigk, Journal of Computational Chemistry **32**, 1456 (2011).

[27] J. N. O'Shea, K. Handrup, R. H. Temperton, A. J. Gibson, A. Nicolaou, and N. Jaouen, The Journal of Chemical Physics **147**, 134705 (2017).

[28] J. N. O'Shea, K. Handrup, R. H. Temperton, A. J. Gibson, A. Nicolaou, N. Jaouen, J. B. Taylor, L. C. Mayor, J. C. Swarbrick, and J. Schnadt, The Journal of Chemical Physics **148**, 204705 (2018).

[29] J. E. Monat, J. H. Rodriguez, and J. K. McCusker, Journal of Physical Chemistry A **106**, 7399 (2002).